

# Self-Assembled Liesegang Rings of Hydroxyapatite for Cell Culturing

Mervat M. Eltantawy, Mikhail A. Belokon, Elena V. Belogub, Olesia I. Ledovich, Ekaterina V. Skorb,\* and Sviatlana A. Ulasevich\*

A novel method of 3D self-organization of patterns made of biomimetic hydroxyapatite (HA) in agar matrix is reported. The model system involves gradual ion diffusion and phase transitions of calcium phosphates. Herein, HA is precipitated for the first time in the agar gel matrix via single-diffusion gel growth technique to aggregate the inorganic Liesegang rings (LRs). These patterns are formed as periodic structures through precipitation reaction and arise during the reagent diffusion in a polymer matrix. The concentrations of these inner and outer electrolytes, as well as pH and temperature effects on the morphologies, periodicity, stability, and number of LRs, are studied. In this study, the periodic HA Liesegang ring structures (HA LRs) are fabricated via a diffusion-limited aggregation process. These patterns influence the C2C12 cell growth and allow to obtain the patterns formed by the cell tissue. This method can be prospective for the generation of 3D gradients in materials/3D gradient materials generation for studying the interface tissue engineering, systematic cell–biomaterial interaction, as well as for the fabrication of the stimuli-responsive gradients to control/mimic migration of cells during the wound healing.

## 1. Introduction

One of the main aims in material engineering is to develop functional biomaterials based on the specific control of molecular building blocks across length scales. There are numerous examples

of materials with periodic structures and prominent properties. For example, the unique properties of bone and dental enamel come out from its distinct hierarchical structure at different length scales.<sup>[1–3]</sup>

Materials and tissue engineering face a sophisticated challenge to create the architecture of biological tissues in terms of physical and chemical characteristics. Therefore, understanding the mechanism of periodic patterns formation is of great interest for fabricating biomimetic materials.<sup>[4]</sup>

3D nanostructuring of cell-laden biomaterials is solved by bioprinting that makes it possible to obtain the materials that can mimic the native tissue structure. The bio-printed structures are used as biomimetic substrates for the coculturing of different cell lines.<sup>[5,6]</sup>

However, bone reconstruction is complicated because these human tissues have a complex structure of approximately 70% minerals and 30% organic matrix by dry

weight.<sup>[6]</sup> The proper formation and functionalization of bones, teeth, and other hard parts of tissue result from the coordinated crystallization.<sup>[7,8]</sup>

Recent interest in regenerative medicine and developing biomimetic scaffolds stimulated the study for the fabrication of complex cell-laden 4D constructs using bioresponsive materials.


Hydroxyapatite (HA) is of great interest as a promising material for bone implants fabrication. It has been used to design biomaterials for hard tissue repair and replacement due to its excellent biocompatibility as well as its close composition and structure similarity to the main inorganic component of bones.<sup>[9–11]</sup>

The HA ( $\text{Ca}_{10}(\text{PO}_4)_6(\text{OH})_2$ ) with Ca/P value 1.67 finds extensive applications in the biomedical field and reconstructive surgeries due to its bioactivity and biocompatibility.<sup>[12–14]</sup> The HA directly binds to bones and prefers the implant fixation in addition to its special characteristics of nontoxicity, noninflammation, and nonimmunogenicity.<sup>[15]</sup>

The biosorption and osteoconductivity make HA suitable for the synthetic bone substitution as it contacts the bone cells and builds a direct chemical connection between bone tissues and implants. Moreover, HA can be a permanent scaffold for new bone formation via its osteoconduction and resorption properties which oversaturate the local environment with  $\text{Ca}^{2+}$  and  $\text{PO}_4^{3-}$  ions to accelerate the formation of new bones.<sup>[16]</sup>

M. M. Eltantawy, M. A. Belokon, O. I. Ledovich, Prof. E. V. Skorb, Dr. S. A. Ulasevich  
Infochemistry Scientific Center  
ITMO University  
9, Lomonosova str., 191002 St. Petersburg, Russia  
E-mail: skorb@itmo.ru; saulasevich@itmo.ru

Prof. E. V. Belogub  
Federal State Budgetary Institution of Science South Urals Federal Research Center of Mineralogy and Geoecology of the Urals Branch of the Russian Academy of Sciences  
Chelyabinsk District, 456317 Miass, Ilmeny Reserve, Russia

 The ORCID identification number(s) for the author(s) of this article can be found under <https://doi.org/10.1002/anbr.202000048>.

© 2021 The Authors. Advanced NanoBiomed Research published by Wiley-VCH GmbH. This is an open access article under the terms of the Creative Commons Attribution License, which permits use, distribution and reproduction in any medium, provided the original work is properly cited.

DOI: 10.1002/anbr.202000048

Many techniques for HA preparation have been reported including chemical coprecipitation,<sup>[17]</sup> sol–gel process,<sup>[18]</sup> spray pyrolysis,<sup>[19]</sup> hydrothermal synthesis,<sup>[20]</sup> and gel method. Particle size, crystallization grade, and structure of calcium phosphate product are confirmed to dependent on synthesis methods and their technological parameters. Therefore, the properties vary considerably from one route to another.

The ability of HA to form the Liesegang rings (LRs) under slow and controlled conditions in agar matrix can be used as a simplified model system for simulation of the growth in human body.<sup>[21,22]</sup>

Our approach is to develop HA pattern formation using self-organization of calcium phosphate particles in agar matrix. The HA is the most thermodynamically stable calcium phosphate phase under physiological conditions.<sup>[23]</sup> The synthesis of biomimetic HA in vitro is still a difficult task due to the diversity of calcium phosphate polymorphs and their sensitivity to pH and ion concentrations.<sup>[23]</sup> We have chosen the method of precipitation in gel because of the simplicity to study the HA product. The most important reason is that the gel method of crystal growth is highly suitable to provide direct observation of the biomineralization process that resembles to human physiological conditions (cartilage and bone formation, etc.) due to its viscous nature.<sup>[24,25]</sup>

During our study, it has been demonstrated that the structure pattern, number, position, width, and periodicity of the rings are influenced by the system conditions, including pH, temperature, and reagent concentrations.

In this article, we focus on the formation of 3D gradients made of calcium phosphates. The HA patterns crystallization occur in agar hydrogel. We study the cooperative effects of pH and ion concentrations on HA formation. The hydrogel network is an excellent system to study crystallization as agar gel prohibits sedimentation of the precipitates formed, and also prevents the other hydrodynamic effects which could be induced by the sedimentation.<sup>[9]</sup> In our research, HA crystals formed in the presence of agar hydrogel have been prepared, and the effects of obtained apatite on the viability and proliferation of C2C12 have been studied.

## 2. Results and Discussion

The bone mineralization occurs by the ordered deposition of HA crystals in the extracellular matrix consisting of type I collagen and various noncollagenous proteins.<sup>[8–10]</sup> The majority of calcium phosphate compounds are poorly soluble in water, nonsoluble in alkaline solutions but resolvable in acids.<sup>[7,10,26]</sup> The agar solution pH greatly impacts the LR formation, their number, width, and stability of LR. The temperature of the agar solution also has a great effect on the formation of LR; at higher temperatures the number, width, and stability of LR also increase. Another important pattern characteristic is the distance between the HA rings which is also called p-factor. The p-factor usually increases on increasing the distance measured from the junction point of the outer and inner electrolytes (gel/liquid interface). Thus, before seeding the cells we have fabricated the HA patterns and studied the empirical characteristics of the system, including the time law, spacing law, width law, and Matalon–Packeter law.

The nonlinear kinetics explains the LR formation and their characteristic periodic structures from the coprecipitation of the reactant compounds. The periodic precipitation taking place when the local concentrations of diffusion reagents reach the solubility constant of the product results in the pattern structure formation.<sup>[7]</sup> Based on prenucleation and supersaturation of the medium, Ostwald put forward a generally accepted mechanism: nucleating particles deplete their surroundings, which causes a drop in the local level of supersaturation such that the nucleation rate falls in the neighborhood area, leading naturally to a spacing between nucleation regions that gives rise to rings, or bands, depending on the system geometry. At the first stage, the outer electrolyte (1 M CaCl<sub>2</sub>) diffuses in the agar gel with inner electrolyte distributed uniformly in the gel. At the gel/liquid interface, the high supersaturation causes instant precipitation of the first LR by nucleation and crystal growth.

So, the local concentration of the inner electrolyte reduces causing a diffusion flow of the inner electrolyte ions from the adjacent regions followed by its depletion near the precipitated ring.

As a result, there are no new nucleation and precipitation near the formed ring due to the little local concentrations of the inner electrolyte. It lasts until the reaction zone shifts far enough from the ring that the depletion effect of the precipitate abates. At the distance from the first ring, the local concentrations of the outer and inner electrolytes reach the solubility product inducing a new nucleation/precipitation. Thus, the pattern periodic structure is formed due to the repeat of the aforementioned processes.<sup>[7,9]</sup>

The Na<sub>2</sub>HPO<sub>4</sub> solution is mixed with agar solution, and then the final solution is cooled down till agar matrix gelation. Due to this procedure, the Na<sub>2</sub>HPO<sub>4</sub> is incorporated uniformly into agar matrix. The CaCl<sub>2</sub> solution is added after agar matrix gelation (Figure S1, Supporting Information). The calcium ions penetrate through the agar matrix and react with phosphate ions to form periodic calcium phosphate structures that are observed in the several hours after addition of the calcium chloride solution (Figure 1). Within the first day most of the bands appeared and continued their formation during the first few days of the first week of the experiment. Several types of precipitates are possible depending on the concentration of disodium phosphate. The distance between the HA rings, the so-called p-factor, depends on the concentration of the solutions from which the precipitation process takes place. As shown in Figure 1, an increase in the sodium phosphate concentration of 0.02 to 0.075 mol L<sup>−1</sup> leads to a decrease in the p-factor value and consequently, the distance between the rings. Both width of HA rings and the time of their appearance decrease by increasing the inner electrolyte concentration. The number of rings increases on increasing the inner electrolyte concentration. It should be mentioned that number of rings, transformation, and crystallization increased by increasing the inner electrolyte concentration. The rings' stability increased on decreasing the inner electrolyte concentration. All these effects are represented as a comparison between two systems having the same conditions of pH, temperature, and outer electrolyte concentration, and only differ in the inner electrolyte concentration (Figure 1, 2).

The HA LR formed within the concentrations, as shown in Figure 2a. The concentration of both outer and inner electrolytes

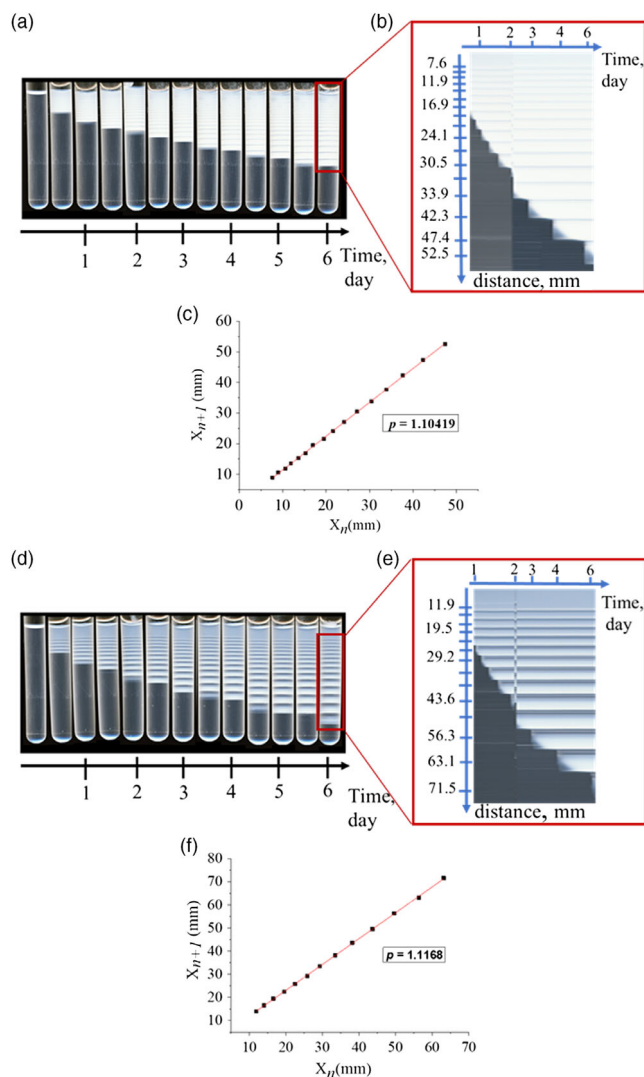


**Figure 1.** A comparison between two systems prepared at the same conditions of pH, temperature, and outer electrolyte ( $\text{CaCl}_2$ ) concentration of  $1 \text{ mol L}^{-1}$ . The concentration of the inner electrolyte ( $\text{Na}_2\text{HPO}_4$ ) was varied from  $0.075 \text{ mol L}^{-1}$  in the a–c) upper system till  $0.02 \text{ mol L}^{-1}$  in the d–f) lower system. The inner electrolyte concentration affects the LRs morphology, number of rings and periodicity including the width of rings, the distance between them, and the speed of their formation. a,d) Time frames of LRs appearance, b,e) Kymogram, and c,f) determination of p-factor which decreases by increasing the inner electrolyte concentration and the rings grow closer.

impacts the LR morphology and periodicity, including the width of rings, time of ring appearance, stability, number of rings, transformation, and crystallization. The types of calcium phosphate precipitates are shown in Figure 2, which is a summary of the concentration experiments explaining different patterns: bands, precipitate, no precipitate in zones named I, II, and III, respectively (Figure 2b,c). Three types dense thick LRs precipitates of are obtained using  $1 \text{ M CaCl}_2$  solution and varying the concentration of sodium phosphate solutions from  $0.005$  to  $0.3 \text{ mol L}^{-1}$ .

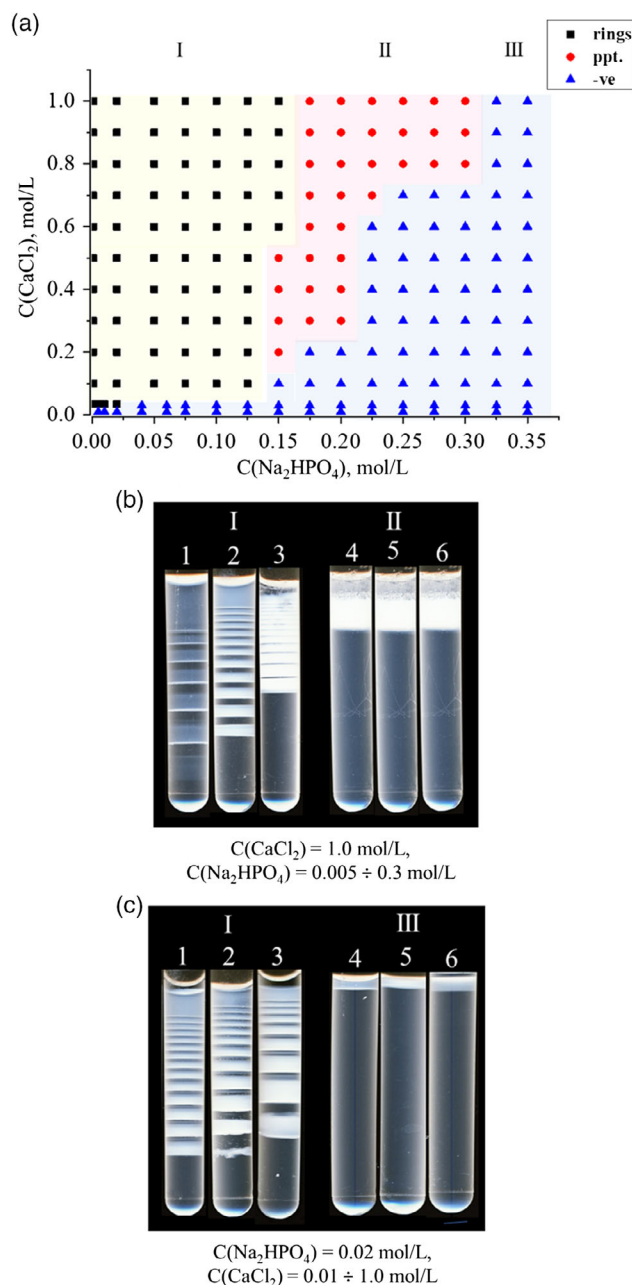


**Figure 2.** a) The influence of different inner and outer electrolyte concentrations on the precipitation behavior. The resulted patterns (bands, precipitate, no precipitate) are shown in zones named I, II, and III, respectively; black squares represent zone (I) and stand for the LRs formation. Red circles represent zone (II) and indicate constant precipitate. Blue triangles represent zone (III) and mean no precipitate. b) Visualization of zone (I) and zone (II). The LR in zone (I) and the precipitate in zone (II) are from tubes obtained at constant concentration of outer electrolyte ( $\text{CaCl}_2$ ) equalled to  $1 \text{ mol L}^{-1}$  and variable concentration of  $\text{PO}_4^{3-}$  in a range of  $0.005 \text{ mol L}^{-1}$  (tube 1),  $0.02 \text{ mol L}^{-1}$  (tube 2),  $0.075 \text{ mol L}^{-1}$  (tube 3),  $0.2 \text{ mol L}^{-1}$  (tube 4),  $0.25 \text{ mol L}^{-1}$  (tube 5), and  $0.3 \text{ mol L}^{-1}$  (tube 6). c) Visualization of zone (I) and zone (III). The LR in zone (I) and the no precipitate in zone (III) are from tubes obtained at constant concentration of inner electrolyte ( $0.02 \text{ M Na}_2\text{HPO}_4$ ) and variable concentration of  $\text{Ca}^{2+}$  in a range of  $1 \text{ mol L}^{-1}$  (tube 1),  $0.3 \text{ mol L}^{-1}$  (tube 2),  $0.1 \text{ mol L}^{-1}$  (tube 3),  $0.01 \text{ mol L}^{-1}$  (tube 4),  $0.02 \text{ mol L}^{-1}$  (tube 5), and  $0.03 \text{ mol L}^{-1}$  (tube 6).

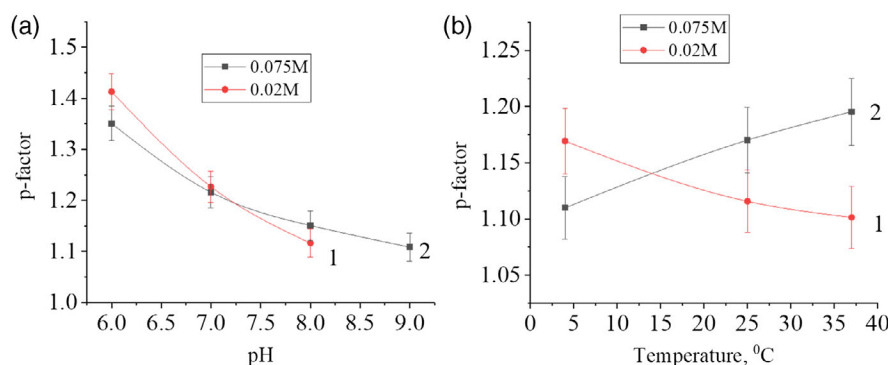


**Figure 3.** a) The influence of pH value on the p-factor. The pH increase causes the decrement of the p-factor regardless the concentrations of the electrolytes. b) The effect of temperature on the p-factor. The temperature change has different impacts on LRs p-factor according to its electrolyte concentrations. The p-factor decreased at higher temperatures and inner electrolyte concentration lower than  $0.02 \text{ mol L}^{-1}$ . It increased on increasing the temperature when inner electrolyte concentration is higher than  $0.075 \text{ mol L}^{-1}$ .

It should be mentioned that the LRs p-factor depends on the concentration of sodium phosphate. The higher the concentration of sodium phosphate, the lower the p-factor value is. There are no LRs formation when concentrated solutions of sodium phosphate ( $>0.3 \text{ mol L}^{-1}$ ) are used (Figure 2b).

At the second stage, a system with a constant concentration of sodium phosphate equal to  $0.02 \text{ mol L}^{-1}$  has been tested with  $\text{CaCl}_2$  solutions of different concentrations. The concentration of calcium chloride was in a range of  $0.01\text{--}1.0 \text{ mol L}^{-1}$  (Figure 2c, zone I). As shown earlier, the formation of LRs is not observed at the increase in  $\text{CaCl}_2$  and  $\text{Na}_2\text{HPO}_4$  concentrations (Figure 2c, zone III). In this case, calcium phosphate

precipitates as a powder. The decrease in  $\text{CaCl}_2$  concentration leads to the increase in the p-factor. The crystallization of LRs is accelerated at the higher concentration of the inner electrolyte ( $\text{C}(\text{Na}_2\text{HPO}_4) > 0.04 \text{ mol L}^{-1}$ ). For example, the crystallization of LRs is observed on the third day, while it is not observed in the systems with lower concentrations of  $\text{Na}_2\text{HPO}_4$  ( $<0.04 \text{ mol L}^{-1}$ ) even till the end of the third week of the experiment. In addition, the dependence of the LRs p-factor on the pH value and the temperature of the precipitation solution was investigated (Figure 3).

The HA LRs do not assemble in the agar matrix at pH in a range of 3–5 because HA formation is more favorable at pH

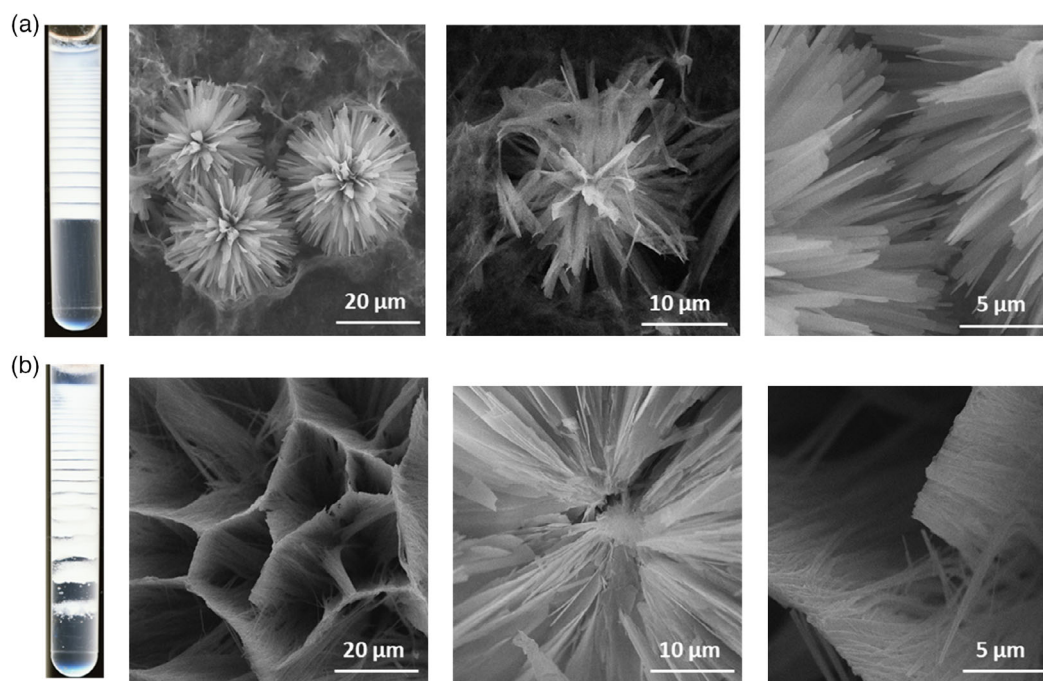


**Figure 4.** SEM images of the calcium phosphate powder obtained from the agar gel after washing and drying: a) platy crystals grown in a tube at temperature  $25^\circ\text{C}$  and pH 9. b) Continuous fibrous network formed by the porous crystals. The network was formed under physiological conditions (pH = 7, the temperature =  $37^\circ\text{C}$ ). All samples were made using concentration of  $0.075 \text{ M Na}_2\text{HPO}_4$  and  $1 \text{ M CaCl}_2$ .



in a range of 6–10. The pH value and temperature are found to affect how fast the HA crystals appear. The lower the pH value, the faster was the crystals' formation. For example, the HA LRs appear immediately within hours at pH of 5.5–6.0. The LRs appeared at the pH = 7.0 within 2 days and after 3–4 days at pH of 8.0–9.0. These results were observed in a system contained  $0.075 \text{ mol L}^{-1}$  of  $\text{Na}_2\text{HPO}_4$  and  $1 \text{ mol L}^{-1}$   $\text{CaCl}_2$  at  $25^\circ\text{C}$  (Figure 3b).

Faster crystals formation is also observed at lower temperatures; the crystals appear immediately within hours at  $4^\circ\text{C}$ , but their appearance is slower at  $25^\circ\text{C}$  for almost within 3 days, and at  $37^\circ\text{C}$  no crystals at all are formed even after the third week (Figure 3b). These results are observed in the same system contained  $0.075 \text{ mol L}^{-1}$   $\text{Na}_2\text{HPO}_4$  and  $1 \text{ mol L}^{-1}$   $\text{CaCl}_2$  at pH 9.0. Thus, changes in the gel pH and temperature not only affect the number and pattern of LRs formation but also the periodicity and speed of the HA transformation and the crystallization appearance. As the pH value increases, the p-factor decreases for both concentrations of sodium phosphate. When the temperature varies from 4 to  $37^\circ\text{C}$ , the p-factor increases in the case of more concentrated solutions of sodium hydrogen phosphate ( $>0.04 \text{ mol L}^{-1}$ ) and decreases in less concentrated solutions ( $<0.04 \text{ mol L}^{-1}$ ). The increase in the p-factor may be explained

by the increase in the calcium chloride diffusion rate through the agar matrix.

Figure 4a shows scanning electron microscopy (SEM) images of calcium phosphate particles grown in 0.4 wt% agar matrix containing  $0.075 \text{ mol L}^{-1}$  of  $\text{PO}_4^{3-}$  at  $25^\circ\text{C}$  (pH = 9). In Figure 4a, the rounded conglomerates of acicular crystals are shown. The average size of the conglomerates is about  $30 \mu\text{m}$ . The deposition of HA LRs at the same concentration but pH = 7 at  $37^\circ\text{C}$  leads to the formation of the porous structure of calcium phosphate rings. This structure is also consisted of elongated needle crystals (Figure 4b).

We fabricate the structure at the pH of 7.4 using phosphate buffer for cell experiments to avoid the cell apoptosis. The X-ray diffraction (XRD) analysis of calcium phosphate powders collected from different levels of the tube with LRs has shown that HA deposits at the beginning of the experiment (Figure 5a, curve 2), while at the bottom of the tube (the end of the experiment) there is a phase of calcium hydrogen phosphate hydrate.<sup>[27,28]</sup> Different phases could be obtained due to the  $\text{Ca}^{2+}$  gradient occurred during the diffusion of the certain volume of  $\text{CaCl}_2$  through the agar gel. It is known that HA forms at the Ca/P ratio of 1.67.<sup>[26]</sup> The decrease in the Ca/P ratio leads to the formation of acidic calcium phosphates.<sup>[26]</sup>

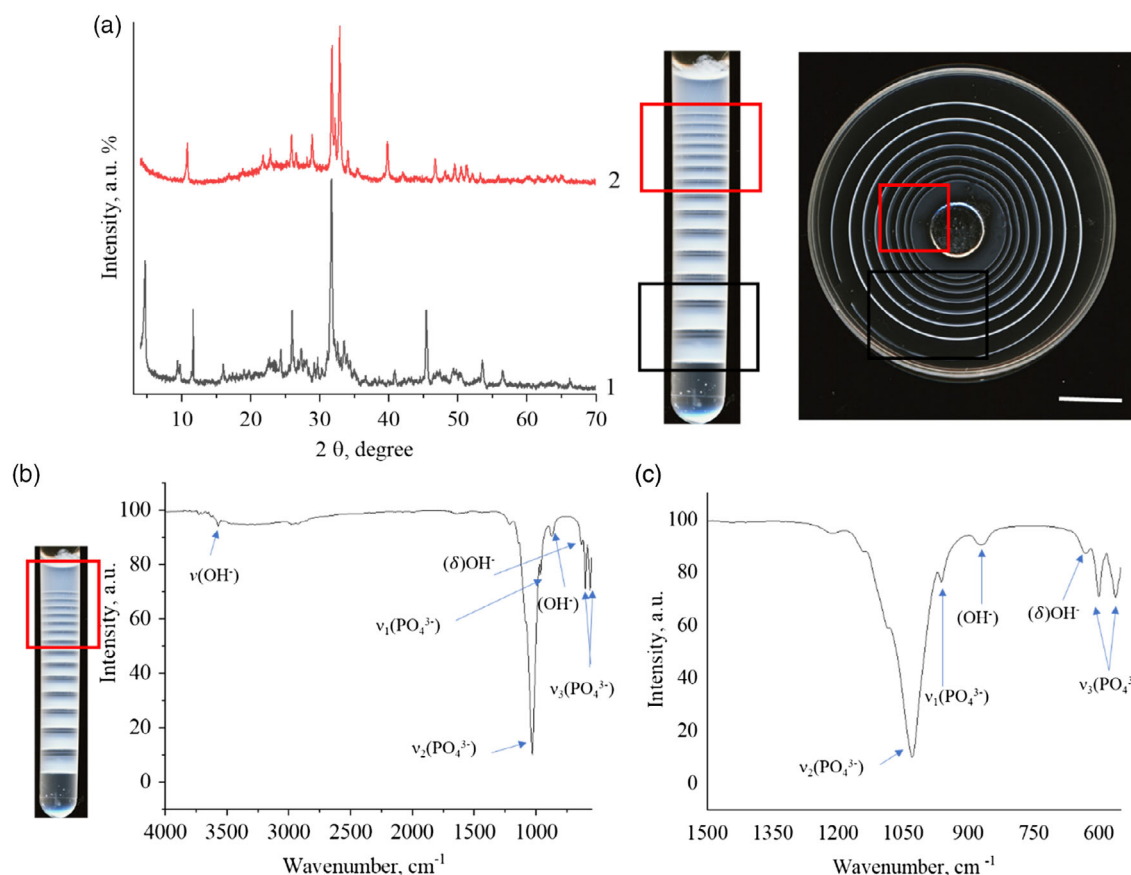


**Figure 5.** a) XRD pattern of the powder obtained from different rings; the rings close to the  $\text{Ca}^{2+}$  reservoir contained HA (curve 2) and those away from  $\text{Ca}^{2+}$  showed TCP (curve 1). The inset shows the photo of the Petri dish with two regions. The scale bar is 1 cm. b) The FTIR spectrum of the bands for the biphasic calcium phosphate powder extracted from the gel after its washing and drying.

**Table 1.** Comparison of the bands observed in the FTIR spectra of samples with the literature data.

Assignments	Vibrational frequency [ $\text{cm}^{-1}$ ]	References
O—P—O bending	562	568, <sup>[30]</sup> 560–600 <sup>[36–38]</sup>
O—P—O bending	601	601, <sup>[30]</sup> 602 <sup>[39]</sup>
( $\delta$ ) O—H	631	635, <sup>[30]</sup> 630 <sup>[36]</sup>
O—H stretching of $\text{HPO}_4^{2-}$	868	875 <sup>[36,37]</sup>
P—O Symmetric stretching	962	960 <sup>[30,36,37]</sup>
P—O Asymmetric stretching	1031	1100–1000 <sup>[30,38]</sup>
( $\text{H}_2\text{O}$ )	1650	1640, <sup>[30]</sup> 1650 <sup>[37]</sup>
O—H Stretching	3571	3572, <sup>[30]</sup> 3570 <sup>[39]</sup>

A similar tendency is also observed for calcium phosphate LRs formed in Petri dishes. There is HA formation near the center of Petri dish where the initial concentration of calcium chloride is higher. At the edge of Petri dish, the concentration of calcium chloride is depleted, and the formation of acidic calcium phosphates is observed. To eliminate this problem, we can use a system in which calcium is supplied continuously until it diffuses throughout the volume of the test tube or Petri dish. In this case, HA is formed. The attenuated total reflectance and Fourier transform infrared (ATR-FTIR) spectra of the calcium phosphate LRs formed in agar matrix containing  $0.02 \text{ mol L}^{-1}$  of  $\text{PO}_4^{3-}$  at the pH 9.0 after addition of  $1 \text{ mol L}^{-1}$   $\text{Ca}^{2+}$  are shown in Figure 5b,c and the assignments are listed in Table 1. There are two characteristic bands around  $562$  and  $601 \text{ cm}^{-1}$  that correspond to  $\nu_4$  (O—P—O) bending mode in spectra. The  $962 \text{ cm}^{-1}$  band in the spectrum is corresponded to  $\nu_1$  (P—O) symmetric stretching and the peak in the range of  $1100$ – $1000 \text{ cm}^{-1}$  is assigned to  $\nu_3$  (PO) antisymmetric stretching mode. These bands designate the characteristic structure of  $\text{PO}_4^{3-}$  polyhedrons in the apatite lattice. A band attributed to  $\text{OH}^-$  groups ( $\delta$ ) and a band of ( $\text{OH}^-$ ) stretching of  $\text{HPO}_4^{2-}$  are observed at  $631$  and at  $868 \text{ cm}^{-1}$ , respectively. Furthermore, the main hydroxyl vibration  $\nu$  ( $\text{OH}^-$ ) is observed at  $3571 \text{ cm}^{-1}$ . The band  $1640 \text{ cm}^{-1}$  ( $\text{H}_2\text{O}$ ) corresponds to water absorption during the synthesis process.<sup>[29,30]</sup>

It should be noted that the HA formation is observed in systems with a constant supply of calcium chloride solution at pH 7.0 and 9.0. No significant difference in IR spectra is observed for powders obtained at  $4$ – $25^\circ\text{C}$ . The presence of carbonate groups is observed in ATR spectrum of calcium phosphate formed at  $37^\circ\text{C}$  (not shown here).

In this article, we propose an alternative method for gradient fabrication. Our method allows to form the periodic ordered rings based on calcium phosphates (Figure 6; Video S1, Supporting Information). The formation of LRs made of HA is performed in a 6-well plate in agar matrix prepared using phosphate buffer (pH 7.4). To increase the content of phosphorus in the system to the stoichiometric ratio of 1.67 corresponding to HA, the amount of sodium phosphate is also added in the agar. After the agar gelation,  $1 \text{ M}$   $\text{CaCl}_2$  solution is dropped to the system. Calcium ions gradually diffuse through the agar hydrogel matrix, leading to the

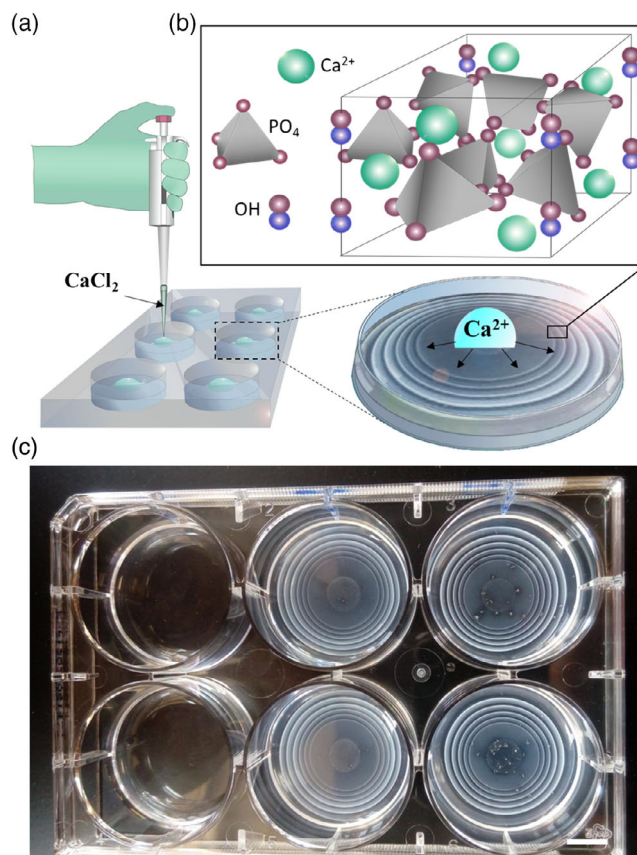


**Figure 6.** Schematic description of the LRs fabrication methodology for cell experiments. a) The preparation of HA Liesegang rings in PBS in 6-well plate, the well diameter is of  $1 \text{ cm}$ . b) The HA chemical structure. c) The rings after their formation in the 6-well plate and the agar control to be incubated with the cells in the culturing media.

formation of calcium phosphates, which are deposited in intermittently ordered rings that are similar to the structure of bone osteons.

Thus, using this system, we can easily and relatively quickly form patterned substrates for cell seeding.

Before experiments with cells, the cytotoxicity of as-prepared calcium phosphate patterns is estimated. We fabricated HA rings in agar at pH 6.5 and 7.2. Then the samples were seeded with cells at the concentration of  $6 \times 10^5 \text{ cells cm}^{-3}$  and cultured for 3 days as usual. Next, we added a solution of 3-(4,5-dimethylthiazol-2-yl)-2,5-diphenyl-tetrazolium bromide (MTT) to the samples and cultured it for 3 h. Then, the medium was removed, and the samples were washed with a phosphate buffer solution (PBS). The formed formazan crystals were dissolved in dimethyl sulfoxide (DMSO). According to the MTT test, formazan crystals were formed both on the control samples and on the samples with rings. However, higher optical density was observed for samples with HA rings formed in PBS buffer. Thus, we can assume high vital activity of cells on our samples. It should be noted that visually formazan crystals formed mainly on the ordered patterns of calcium phosphates. The MTT test results are shown in Figure S2, Supporting Information.

The distance between HA rings is  $\approx 100\ \mu\text{m}$  (Figure 7b,c) and it increases from one ring to another. The rings have porous structure (Figure 7c); the pore size is shown not to exceed  $10\ \mu\text{m}$ . To investigate the influence of the calcium phosphate gradients on the cell growth, we divide the sample into several regions. First region (Figure 7a, S2a, Supporting Information) is located in the center of the calcium phosphate rings (marked with a green square), while the second region is located between rings (Figure 7a, S2b, Supporting Information) and marked with

a green square. The third region is space without any pattern, and is taken as a control one. In Figure 7e–i, we can see that cells on the prepared samples with HA patterns prefer to attach and grow around the LR. However, cell density on agar and on the place between the rings is much lower. This could be explained by two phenomena. At first, C2C12 prefers the rigid surfaces,<sup>[31–34]</sup> while the agar surface is quite soft. Deposition of calcium phosphate may increase the stiffness of the sample surface as was shown in the similar case with MC3T3-E1 cells in work.<sup>[35]</sup> The

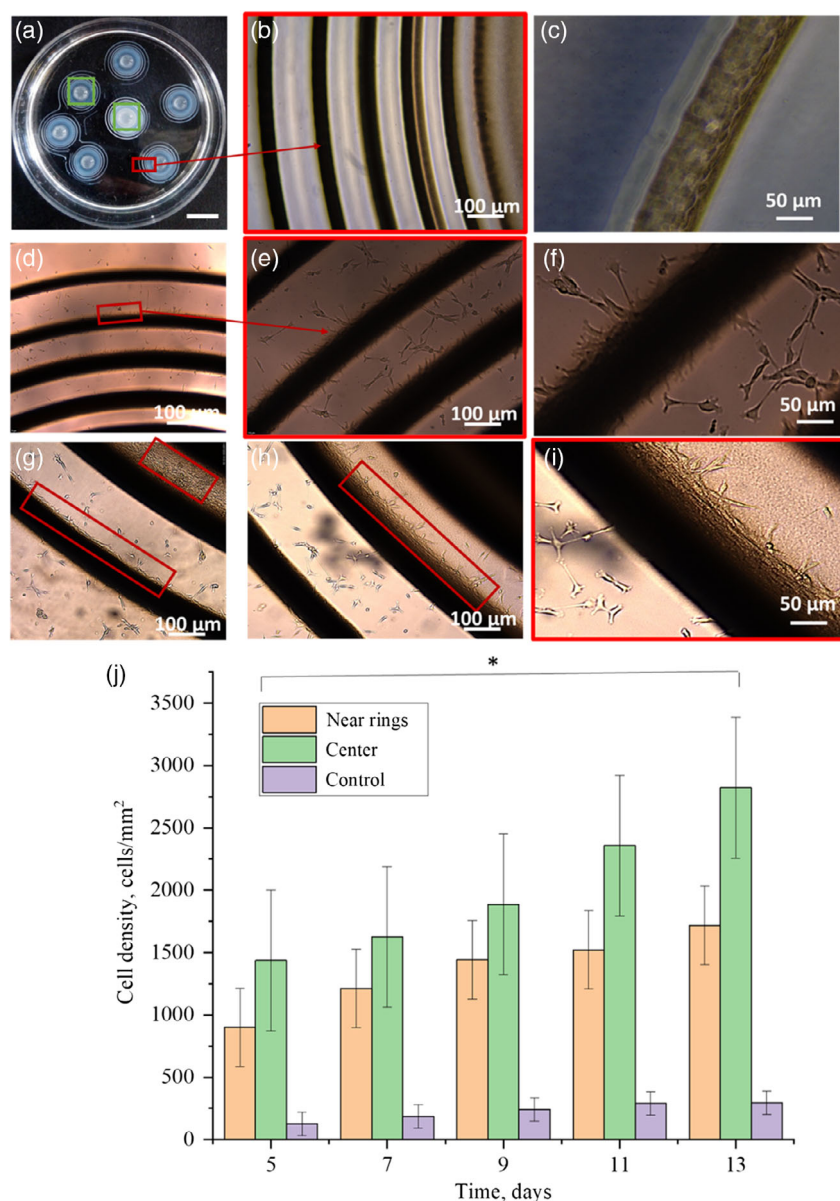


**Figure 7.** a) The photo of the Petri dish with the formed HA LR in PBS agar matrix using  $0.02\ \text{M}\ \text{Na}_2\text{HPO}_4$  and  $1\ \text{M}\ \text{CaCl}_2$ . The scale bar is 1 cm. The green square shows the region in the LR center. The red square shows the region between rings. b) Fluorescent microscope image showing the initial calcium phosphate rings. c) Fluorescent microscope image focusing on the part of calcium phosphate ring. d,e) Optical microscope images of the C2C12 cells grown on the rings after 7 days of cultivation. f) Optical microscope image revealing the preferable growth of C2C12 cells on the calcium phosphate rings. g–i) Optical microscope images of the C2C12 forming tissues on the rings after 9 days of cultivation. j) Histogram of C2C12 cell density on different areas of the sample during 17 days of cell cultivation, error bars represent standard deviation. Three samples were tested per each area type and three independent experiments were conducted.  $*p < 0.05$ ,  $n = 3$ .



second factor is HA that may serve as a source of the  $\text{Ca}^{2+}$  and  $\text{PO}_4^{3-}$  for cells and accelerates their proliferation.<sup>[36–39]</sup> The cell density is about 30 times higher on the HA rings compared with the agar gel taken as a control one (Figure 7j). The increased proliferation of cells is also observed near the rings (Figure 7e–i). Several techniques with various dyes that preferentially bind with DNA are applied to detect cells and to confirm that within first 1–5 days cells prefer to grow on calcium phosphate rings. We use these dyes due to the fact that our system consists of agar and calcium phosphates that also bind very quickly with the dyes used for cell staining. As a result, we have obtained a picture with very noisy background (not shown here). The most interesting results were obtained using propidium iodide (PI), which binds with DNA in the cell nuclei. In **Figure 8b**, we can see the cells growing on the calcium phosphate patterns, while there are no cells in the space between rings. The presence of cells on the surface of the LRs is also confirmed by the formation of the LRs in an ultrathin agar layer, which results in the formation of a translucent HA rings. We fabricated patterns of calcium phosphates in a thin

agar layer on a glass slide. The cell shadows were observed on these samples.

To further confirm that cells prefer to grow on the calcium phosphate rings surface, the samples were stained as follows. Samples were placed in 6-well plates and seeded with cells according to the protocol described earlier. After fixing and staining the cells, the samples were flipped so that we could see the cells grown on the surface of the nontransparent rings. In **Figure 8c–e**, the cell nuclei were stained with PI. These nuclei are located on the shadows of the HA rings, whereas in the areas between the rings, cells do not grow such intensively. Thus, we can observe gradients of cell density on the sample surface. Moreover, the gradients of cell density repeat the previously formed pattern of calcium phosphates. At the same time, the calcium phosphate patterns are resorbed in the process of cells vital activity. Therefore, we can see a pattern made of cell tissue.

The presence of cells on the HA surface was also confirmed by the technique in which the C2C12 cells are fixed on the surface and detached from the sample surface using Versene solution. In

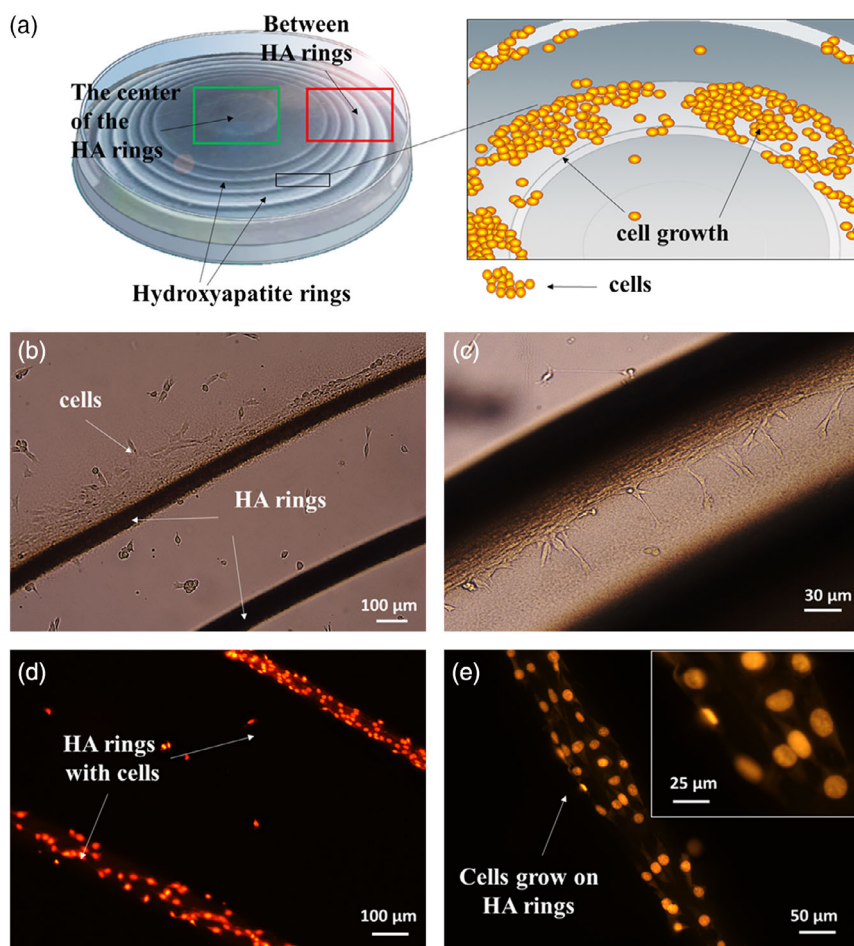


**Figure 8.** a) The schematic illustration of the preferred cell growth on the HA LR. The green square shows the region in the center of calcium phosphate rings. The red square shows the region between rings. The calcium phosphate rings could act as  $\text{Ca}^{2+}$  reservoirs and influence cell growth. b,c) The optical image of the cells grown near the calcium phosphate rings after 7 days of cultivation. d,e) The confocal image of the cells grown on the calcium phosphate rings after 5 days of cultivation. The nuclei are stained using PI at the fluorescent excitation maximum of 493 nm, and an emission fluorescent maximum of 636 nm.



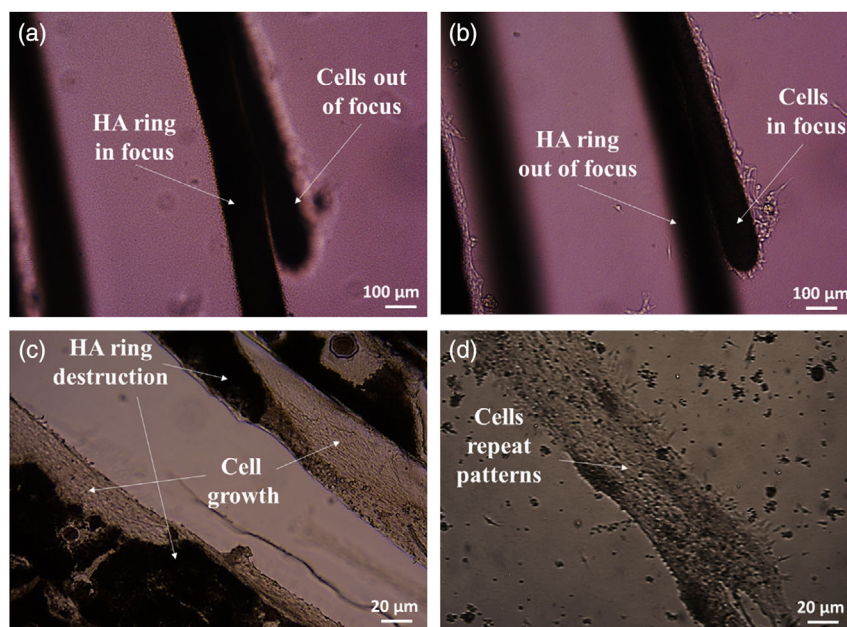


**Figure 9.** The 3D cells gradient formation. a,b) Optical images of cell tissue grown on the calcium phosphate ring. During the staining, the cell tissue grown on the ring was separated. The images were obtained at different focuses. c,d) The optical photo of the partially destroyed HA LRs and the cells immobilized on it and repeated the rings pattern during their proliferation.

**Figure 9a**, we observe the HA rings and a dark stripe out of the focus above them. **Figure 9b** shows that this stripe is formed by cell tissue and has grown on the HA ring in 7 days of cultivation. The same effect is also observed when studying cell cultivation in the same area of the HA ring.

Observing the same place on the sample, we noted that the calcium phosphate pattern dissolves over time, and there is an intensive cell proliferation on this place leading to tissue formation. As HA dissolves, the cell tissue grows and repeats the initial pattern of HA ring (**Figure 9c,d**). At the same time, nonsignificant cell growth is observed on agar surface and between the LRs, while instead of rings, cell tissue has already been organized in the form of rings. **Figure 9d** demonstrates the cellular tissue formed into a strip in place of the destroyed ring. Thus, the resulting structures are promising substrates for studying bone formation and cell proliferation. The obtained substrates can also be an alternative to 3D bioprinting and can be used for the formation of cellular structures and patterns. The resulting systems may find their application in Lab-on-Chip and smart coatings technologies.

### 3. Conclusion

This work demonstrates a method of 3D multiscale self-organization of periodic patterns from HA for the first time. The biomimetic synthesis of HA with bone-like morphology occurs under physiological conditions using agar hydrogel matrix containing sodium phosphate. The periodic HA rings assembled by elongated needle-shaped nanocrystals are obtained. The agar hydrogel matrix is able to mediate the deposition of the HA inside the 3D agar network as well as influence

the self-assembly of HA precipitation. The effect of various factors, such as the concentrations of inner and outer electrolytes, pH value, and temperature, on the LR morphologies has been studied. Biocompatibility of HA periodic patterns has been studied in vitro using C2C12. The unique effect of cell tissue formation on the HA rings has been shown. It is revealed that C2C12 cells repeat the initial pattern of the HA rings. Thus, the developed method of 3D self-organization of cell growth can be a prospective method for 3D gradient materials engineering. The presented system has great potential in biomedical field and could be used in bone tissue engineering.

## 4. Experimental Section

### 4.1. HA Patterns Fabrication

Calcium phosphate precipitation was obtained by the diffusion of  $\text{CaCl}_2$  through the agar matrix containing  $\text{Na}_2\text{HPO}_4$  (inner electrolyte). The  $\text{Na}_2\text{HPO}_4$  was dissolved in 10 mL agar solution and stirred under the heating until the mixture became homogeneous. Then, this solution was added into a tube (15 cm length, 1 cm diameter) and cooled down at room temperature  $25^\circ\text{C}$  till the agar gelation without any disturbance. The calcium chloride solution (the outer electrolyte) was poured to the tubes with gelled agar and  $\text{Na}_2\text{HPO}_4$ . Visual observations of the precipitation were recorded using a high-resolution scanner that took images every 2 min during 24 h.

The concentrations of the inner and outer electrolytes were varied to investigate all the possible types of the precipitate. The influence of the pH value and temperature on the LR formation was also examined. The pH was varied in a range of 3–9

to study the LR formation, as different phases of calcium phosphates deposit at a certain pH. The glacial acetic acid was added dropwise into the tube to adjust the acidic pH, and LR formation was observed.

Temperature influence on the LR was tested at +4 to 7 °C. The tubes with as-prepared reagents were stored in a thermostat at a constant temperature within 2 weeks.

#### 4.2. Physical and Chemical Characterization of HA Patterns

The prepared LR were separated from agar and washed in hot distilled water 5 times to dissolve the rest of the agar. The rinsed powder was dried at 60 °C in air till the constant mass. The dried powder of calcium phosphates obtained from different parts of the tube (top, middle, and bottom) and Petri dish (center, near rings, distant rings) were characterized by different techniques.

**ATR-FTIR:** The ATR-FTIR spectra were recorded to study the phase content of the calcium phosphate powders using Nicolet iS5 FTIR Spectrometer (Nicolet Instrument Corporation, USA). The powders were placed directly on the ATR crystal made of ZnSe (refractive index  $n = 2.4$ ). The spectra were performed in a range of 400–4000  $\text{cm}^{-1}$  at a resolution of 4  $\text{cm}^{-1}$ . Each spectrum was built after 32 scans.

The OMNIC software was used to collect and analyze the IR spectra.

**XRD Analysis:** The powder samples were investigated by the X-ray phase analysis (Shimadzu XRD-6000 diffractometer, Cu  $K\alpha = 1.5405 \text{ \AA}$ ). The spectra were recorded using Powder X program. Diffraction spectra were measured at a range of  $2\theta$  from 5° to 70° at a rate of 1°  $\text{min}^{-1}$ . The spectra were analyzed for the presence of main reflections of HA and tricalcium phosphate (TCP).

**SEM:** The powder samples were sputtered with carbon to create the conductive layer and to avoid charging effects. The surface morphology of the powder particles was examined using a Tescan VEGA3 Scanning Electron Microscope (Tescan, CZE). The operating voltage was 10 kV. The Tescan Essence software has been used.

#### 4.3. in Vitro Biocompatibility Study

**Cells Culturing:** The C2C12 cells were purchased from Sigma-Aldrich. The cells were cultivated into flasks with Dulbecco's Modified Eagle's medium (DMEM) containing 10% fetal bovine serum and 1% antibiotics (5000 units per 1 mL of penicillin G and 5  $\text{mg mL}^{-1}$  streptomycin). The medium was changed every 3 days.

**Cells Seeding on the Calcium Phosphate Rings:** The LR were prepared as mentioned earlier. The 0.4 wt% agar solution containing 0.02  $\text{mol L}^{-1}$   $\text{Na}_2\text{HPO}_4$  was prepared using PBS buffer (pH = 7.4) as a solvent instead of water. The Petri dishes were used instead of cylindrical tubes. The 1 M  $\text{CaCl}_2$  solution was dropped on the surface of the agar gel. The drop volume was 10  $\mu\text{L}$ . Every stage was performed in sterile conditions. The cells were seeded after nine passages onto the biomaterial surfaces at the density of  $6 \times 10^5 \text{ cells cm}^{-2}$ .

The cells were left undisturbed in an incubator to allow their attachment to the rings and to grow using the same culture medium (DMEM containing 10% fetal bovine serum and 1% antibiotics [5000 units per 1 mL of penicillin G and 5  $\text{mg mL}^{-1}$  streptomycin]). The samples with cells were cultured in a humidified atmosphere (95% air and 5%  $\text{CO}_2$ ) at 37 °C for 17 days. The medium was changed every 2–3 days. Control samples were performed using only 0.4 wt% agar prepared in PBS.

**MTT-Assay:** The samples were cultivated in a humidified incubator at 37 °C with 95% air and 5%  $\text{CO}_2$  for 3 days. The MTT solution was prepared by dissolving the 3-(4,5-dimethylthiazol-2-yl)-2,5-diphenyl-tetrazolium bromide in a PBS at a concentration of 1  $\text{mg mL}^{-1}$ .

At the 4th day, the medium was aspirated and replaced with PBS, and 50  $\mu\text{L}$  of MTT solution was added to each well. The 12-well plate was incubated for another 6 h at 37 °C. In 6 h, the MTT solution was removed carefully, and samples were washed 3 times in PBS.

The DMSO was added to each well to dissolve the formed formazan crystals. The plate was incubated for next 3 h at stirring by hand to enhance the dissolution of blue formazan.

The optical density of each well was measured using an automatic microplate reader (iMark, Bio-Rad Laboratories, USA) with a 670 nm reference wavelength and 570 nm test wavelength.

**Cells Staining:** For staining experiments, cells culturing on the LR surfaces were done on sterile transparent cover glasses.

After 5 days, acridine orange (AO) staining was used to show cell agglomeration on the rings surface. Then, the culture medium was taken away. The cells were fixed in 4% PFA for 5 min. The 0.1% Triton X-100 solution was used to reach the cell permeability. After three washes with PBS, cells were stained by 0.01% AO (Sigma, USA) for 15 min in dark place at 37 °C and then observed by fluorescence microscopy (LEICA DMi 8, USA) and LEICA software.

For staining with PI, the cells were fixed on the sample surface in 70% ethanol–water solution for 15 min. Then, the samples were quickly washed 3 times with PBS.

The 2 mL of distilled water was added in each well and 20  $\mu\text{L}$  of PI solution at a concentration of 1  $\text{mg mL}^{-1}$  was also added. The samples were stored in the dark at +4 °C for 20 min. Then, the samples were washed quickly 3 times with distilled water.

The samples were flipped and examined using fluorescent microscope, the fluorescent excitation maximum was 493 nm, and the emission maximum was 636 nm.

**Cells Statistics:** Three zones on the sample surface were chosen to study the cell density on the material with a calcium phosphate gradient. Zone 1 is a center of the formed pattern (rings). Zone 2 is a space near the rings or between the rings. Zone 3 is a control one containing an agar layer without calcium phosphate rings. All samples were prepared under the same conditions.

Six images were taken in each zone in different places. The number of cells was processed using the ImageJ program. The mean cell density and standard deviation were calculated. The data were presented as mean values  $\pm$ SD. Samples with cell density exceeding the standard deviation were evaluated, and the experiment was done again.

The patterns and 3D gradients of calcium phosphates were grown on the cover glass squares. The edge length is 2 cm;

the sample area is 4 cm<sup>2</sup>. The sample size for each statistical analysis was the same.

Statistical relevance of the mean cell density during each experiment was calculated by one-way ANOVA, using Excel descriptive statistics. Pairwise comparison of inter experiment data was made with two-way ANOVA or *F*-test of the equality of two variances (ANOVA).

Standard errors in the data points were determined at the 95% confidence interval and  $p \leq 0.05$  within each experiment was considered as significant. All experiments were done in triplicate and were repeated three times.

## Supporting Information

Supporting Information is available from the Wiley Online Library or from the author.

## Acknowledgements

The authors acknowledge RSF grant no. 19-79-10244 for the financial support. ITMO Fellowship and Professorship Program 08-08 is acknowledged for infrastructural support. The authors are grateful to Anastasia Nenashkina for her nice scheme drawings.

## Conflict of Interest

The authors declare no conflict of interest.

## Data Availability Statement

Research data are not shared.

## Keywords

C2C12 cells, calcium phosphates, Liesegang rings, periodic structure patterns, self-assembly

Received: October 16, 2020

Revised: February 10, 2021

Published online:

- [1] S. Elsharkawy, M. Al-Jawad, M. F. Pantano, E. Tejeda-Montes, K. Mehta, H. Jamal, S. Agarwal, K. Shuturminskaya, A. Rice, N. V. Tarakina, R. M. Wilson, A. J. Bushby, M. Alonso, J. C. Rodriguez-Cabello, E. Barbieri, A. del Río Hernández, M. M. Stevens, N. M. Pugno, P. Anderson, A. Mata, *Nat. Commun.* **2018**, 9, 2145.
- [2] A. Lotsari, A. K. Rajasekharan, M. Halvarsson, M. Andersson, *Nat. Commun.* **2018**, 9, 4170.
- [3] W. Jiang, D. Athanasiadou, S. Zhang, R. Demichelis, K. B. Kozlars, P. Raiteri, V. Nelea, W. Mi, J. A. Ma, J. D. Gale, M. D. McKee, *Nat. Commun.* **2019**, 10, 2318.
- [4] B. Byambaa, N. Annabi, K. Yue, G. Trujillo-de Santiago, M. M. Alvarez, W. Jia, M. Kazemzadeh-Narbat, S. R. Shin, A. Tamayol, A. Khademhosseini, *Adv. Healthcare Mater.* **2017**, 6, 1700015.

- [5] N. Ashammakhi, A. Hasan, O. Kaarela, B. Byambaa, A. Sheikhi, A. K. Gaharwar, A. Khademhosseini, *Adv. Healthcare Mater.* **2019**, 8, 1801048.
- [6] Y. Shimizu, J. Matsui, K. Unoura, H. Nabika, *J. Phys. Chem. B* **2017**, 121, 2495.
- [7] H. Zhang, K. Zhan, Y. Chen, G. Chen, X. Zhou, J. Liu, M. Wu, H. Ni, *J. Sol-Gel Sci. Technol.* **2014**, 71, 597.
- [8] G. H. Nancollas, W. Wu, *J. Cryst. Growth* **2000**, 211, 137.
- [9] M. P. Ferraz, F. J. Monteiro, C. M. Manuel, *J. Appl. Biomater. Biomech.* **2004**, 2, 74.
- [10] P. Kanchana, C. Sekar, *J. Cryst. Growth* **2010**, 312, 808.
- [11] C. Li, F. Meng, *Mater. Lett.* **2008**, 62, 932.
- [12] M. Vallet-Regí, *Comptes Rendus Chim.* **2010**, 13, 174.
- [13] H. Imai, S. Tatara, K. Furuichi, Y. Oaki, *Chem. Commun.* **2003**, 3, 1952.
- [14] S. Gomes, G. Renaudin, E. Jallot, J. M. Nedelec, *ACS Appl. Mater. Interfaces* **2009**, 1, 505.
- [15] M. Ashok, N. Meenakshi Sundaram, S. Narayana Kalkura, *Mater. Lett.* **2003**, 57, 2066.
- [16] H. Wang, Y. Li, Y. Zuo, J. Li, S. Ma, L. Cheng, *Biomaterials* **2007**, 28, 3338.
- [17] A. Sinha, S. Nayar, A. Agrawal, D. Bhattacharyya, P. Ramachandrarao, *J. Am. Ceram. Soc.* **2003**, 86, 357.
- [18] W. Weng, J. L. Baptista, *Biomaterials* **1998**, 19, 125.
- [19] W. Suchanek, M. Yoshimura, *J. Mater. Res.* **1998**, 13, 94.
- [20] M. Yoshimura, H. Suda, K. Okamoto, K. Ioku, *J. Mater. Sci.* **1994**, 29, 3399.
- [21] P. Kanchana, C. Sekar, *J. Miner. Mater. Charact. Eng.* **2012**, 11, 982.
- [22] F. Peters, M. Eppe, *Zeitschrift für Kardiologie* **2001**, 90, 81.
- [23] Y. Han, T. Nishimura, M. Iimura, T. Sakamoto, C. Ohtsuki, T. Kato, *Langmuir* **2017**, 33, 10077.
- [24] N. Meenakshi Sundaram, E. K. Girija, M. Ashok, T. K. Anee, R. Vani, R. V. Suganthi, Y. Yokogawa, S. N. Kalkura, *Mater. Lett.* **2006**, 60, 761.
- [25] H. Nabika, M. Itatani, *Langmuir* **2019**, 36, 481.
- [26] R. V. Suganthi, E. K. Girija, S. Narayana Kalkura, H. K. Varma, A. Rajaram, *J. Mater. Sci.: Mater. Med.* **2009**, 20, S131.
- [27] J. G. Rabatin, R. H. Gale, A. E. Newkirk, *J. Phys. Chem.* **1960**, 64, 491.
- [28] K. Sakamoto, S. Yamaguchi, M. Kaneno, I. Fujihara, K. Satoh, Y. Tsunawaki, *Thin Solid Films* **2008**, 517, 1354.
- [29] L. Berzina-Cimdina, N. Borodajenko, *Infrared Spectrosc. – Mater. Sci. Eng. Technol.* **2012**, 12, 251.
- [30] A. Paz, D. Guadarrama, M. López, J. E. González, N. Brizuela, J. Aragón, *Quim. Nova* **2012**, 35, 1724.
- [31] N. Brezhneva, E. V. Skorb, S. A. Ulasevich, *Proc. IEEE 7th Int. Conf. Nanomaterials: Applications and Properties* **2017**.
- [32] E. V. Skorb, H. Möhwald, D. V. Andreeva, *Langmuir* **2016**, 32, 11072.
- [33] K. Anselme, P. Davidson, A. M. Popa, M. Giazgon, M. Liley, L. Ploux, *Acta Biomater.* **2010**, 6, 3824.
- [34] P. M. Gilbert, K. L. Havenstrite, K. E. G. Magnusson, A. Sacco, N. A. Leonardi, P. Kraft, N. K. Nguyen, S. Thrun, M. P. Lutolf, H. M. Blau, *Science* **2010**, 329, 1078.
- [35] A. Abalymov, L. Van Der Meeren, M. Saveleva, E. Prikhodzhenko, K. Dewettinck, B. Parakhonskiy, A. G. Skirtach, *ACS Biomater. Sci. Eng.* **2020**, 6, 3933.
- [36] A. Destainville, E. Champion, D. Bernache-Assollant, E. Laborde, *Mater. Chem. Phys.* **2003**, 80, 269.
- [37] S. Raynaud, E. Champion, D. Bernache-Assollant, P. Thomas, *Biomaterials* **2002**, 23, 1065.
- [38] I. Mobasherpour, M. S. Heshajin, A. Kazemzadeh, M. Zakeri, *J. Alloys Compd.* **2007**, 430, 330.
- [39] J. K. Han, H. Y. Song, F. Saito, B. T. Lee, *Mater. Chem. Phys.* **2006**, 99, 235.